USE OF ELASTOMERIC ELEMENTS IN CONTROL OF ROTOR INSTABILITY

Anthony J. Smalley
Mechanical Technology Incorporated (MTI)
Latham, New York 12100

SUMMARY

Elastomeric elements are seeing increasing, successful use in control of unstable rotor vibrations. Elastomers are used both as seals for squeeze film dampers and as dissipative elements in their own right. In either application, their success is dependent upon a correct match between rotor and suspension dynamic characteristics. This paper presents information on the dynamic characteristics of elastomeric supports. Stiffness and damping characteristics for elastomers of various geometries including O-rings, buttons loaded in compression, and rectangular elements loaded in shear are presented. The effects of frequency, temperature, and amplitude are illustrated, as well as the effects of material and geometry. The basis for this data is dynamic component testing. Empirical design methods are illustrated, and several examples are presented where elastomers have successfully controlled both synchronous and nonsynchronous vibrations.

INTRODUCTION

In a number of rotating machinery applications, undesirable vibrations, both synchronous and nonsynchronous, can be controlled by simple elastomeric bearing mounts. Belief in this statement has led to a sustained effort at Mechanical Technology Incorporated (MTI), under NASA funding, to provide the necessary elastomer data to develop the means to apply it, and to demonstrate the vibration control capability of elastomers for rotating machinery. The program approach has been empirical and is directed at answering the questions of the rotor dynamicist who must perform analysis and design synthesis to achieve smoothly running rotors.

Some highlights of available data are presented in this paper together with some illustrations of effective vibration control by elastomeric elements. For more extensive data, the reader is referred to the list of references at the end of the paper.

COMPONENT TESTING

Component dynamic data have been generated by the base excitation resonant mass method, whose main features are shown in Figure 1. A high-capacity electromagnetic shaker applies a sinusoidal motion to the base of an elastomeric spring on which a mass is supported, and accelerometers measure the transmissibility and phase difference between base and mass. Near resonance, these measurements are accurately translated into stiffness and damping of the elastomeric spring.

Various geometries have been tested, including cylindrical buttons in compression; rectangular elements in shear; ring cartridges under radial loading; and O-rings under radial loading. These geometries are illustrated in Figure 2.

In Figure 3, a typical set of test results, covering the frequency range between approximately 100 and 1000 Hz, is presented. These data apply to a rectangular element of Polybutadiene loaded in shear and exhibit small, but acceptable, scatter about a line showing steadily increasing stiffness and damping with frequency. A power law variation of the form $K = A\omega^B$ has been fitted to most data sets.

Shear stiffness of rectangular elements is proportional to sheared area. However, the axial stiffness of cylindrical buttons increases more nearly as the square of the stressed area. Incompressibility of the elastomer causes this effect since any axial deformation of the cylinder must be accompanied by radial deformation to maintain the same volume. Empirical correlations with diameter-to-height ratio for different button sizes are shown in Figure 4.

Stiffness and loss coefficients for O-rings in radial deformation are shown as functions of frequency in Figures 5 and 6. In Figure 5, three different materials are compared: Viton 70, Viton 90, and Buna-N (70 durometer). The two 70 durometer materials show similar stiffnesses, although Viton 70 has a steeper slope. Viton 90 is approximately four times as stiff as the Viton 70. The loss coefficient for Viton 70, at about 0.9, is highest, compared with 0.5 for Viton 90 and 0.3 for Buna-N. Figure 6 shows the striking effects of increasing temperature on dynamic characteristics of Viton 70. The loss in stiffness is severe, and the decrease in loss coefficient even more pronounced; the excellent room temperature damping characteristics of Viton 70 are not fully maintained at the high temperatures which Viton can withstand.

Another important environmental parameters is the dynamic amplitude to which the elastomeric element is exposed as shown in Figure 7 for cylindrical Polybutadiene elements in compression. Stiffness steadily falls with increasing strain, particularly above 0.003, but loss coefficient steadily increases; properly exploited, strain of this material could result in increasingly effective vibration control!

It has been shown convincingly in several test series that the changes in elastomeric characteristics with strain are not solely the result of self-heating Even when temperature rise in the elastomer is negligible, strain effects may be pronounced. However, under sufficiently high strains, elastomers do get hot. A 60° temperature increase is possible, as shown by the centerline profiles in Figure 8.

In Figure 9, the effects of strain on Viton 70 are seen to differ slightly from those observed for Polybutadiene. Both stiffness and loss coefficients of Viton 70 fall with increasing strain! Herein lies a further difficulty in dealing with elastomers: generalities are dangerous!

454

ROTOR DYNAMICS ANALYSIS WITH ELASTOMERIC ELEMENTS

Elastomeric rotor mounts must be matched to the dynamic characteristics of the rotor to give the best possible system dynamic performance. The design analysis and synthesis process are illustrated in Figure 10. Prior to component analysis, the rotor itself is analyzed to determine the optimum support characteristics. Component analysis, within environmental constraints such as temperature and available space, provides either a configuration which meets the desired optimum or a number of compromise configurations which minimize the deviation from optimum. From these alternatives, a final selection of geometry and material is made, and predictions of rotor system performance, with the selected component characteristics, are made. In some cases, the final damper configuration selection may be left to component or system rig test since elastomeric dampers can usually be designed to be readily replaceable.

In Figure 11, typical optimization curves show log decrement for a flexible rotor (a turboshaft engine dynamic simulator) as a function of elastomeric support damping. At first and second critical speeds, 100 lb·sec/in. is a clear optimum for both first and second criticals. The stiffness in this case is 100,000 lb/in., and Table 1 shows the damping which can actually be achieved in a 100,000 lb/in. elastomeric mount at the second critical speed. For Viton 70 and Polybutadiene, the damping will be 38 and 7.2 lb·sec/in., respectively, and the corresponding system log decrements will be 0.31 and 0.075, respectively, compared with the optimum of 0.965. A clear compromise is necessary for either material.

Figure 12 shows how component data are presented in the selection of diameter and height to achieve the desired stiffness of 100,000 lb/in.

APPLICATIONS EXAMPLES

Turboshaft Engine

Figure 13 shows, schematically, a test rotor designed as a dynamic simulator for an advanced, flexible rotor, turboshaft engine. The large disc at one end simulates the power turbine. The rotor runs in ball bearings which are themselves either hard-mounted or mounted in elastomeric dampers. The elastomeric dampers designed for this rig are shown in Figure 14. Around each bearing three groups of three cylindrical buttons support the bearing housing. These individual cartridges could be readily replaced, and several configurations were tested. Variable preload was achieved by means of a preload screw.

Figure 15 shows how elastomer material affects predicted response to unbalance. The higher loss coefficient of the Viton achieves a significantly lower response than Polybutadiene, corresponding to the higher log decrement presented in the previous section. The test data of Figure 16 show how sensitive to unbalance excitation the rotor was when first mounted on rigid metal cartridges. The response at around 20,000 rpm rises sharply to a peak of about nine mils. Figure 17 shows the drastic improvement in dynamic sensitivity when the rotor is flexibly mounted in Viton dampers. The largest response with half a gram of unbalance is less than 3-1/2 mils, and the shape of the response curve is very broad, indicating good system damping. The linear variation in amplitude with

unbalance is also apparent from these curves. It should be noted that the rotor was readily balanced to the lowest vibration curve in Figure 17 with a peak amplitude of only about one-third mil. These results are considered to be strong evidence for the potential benefits of elastomers in controlling flexible rotor vibrations.

Supercritical Power Transmission Shaft

Figure 18 shows, schematically, a test rig designed to evaluate flexible power transmission shafts for helicopter tail rotors. The test shaft was 12 feet long, 3 inches in diameter, with 1/8 inch aluminum walls, and had three critical speeds below 10,000 rpm. The rotor was initially hard-mounted, by means of angularly flexible couplings, from rigid shaft support spindles. Figure 19 shows the sharp response to unbalance at the first critical speed. Limiting amplitudes of about 75 mils peak-to-peak were reached with very small levels of residual unbalance. With great difficulty, the rotor was balanced through this first critical speed, but, as shown in Figure 20, when running at 20 percent above this first critical, the subsynchronous vibration level was almost as high as when negotiating the critical speed and seven or eight times the synchronous amplitude. Violent unstable motion occurred at these and higher speeds and there was no possibility of running the hard-mounted shaft any faster.

A damper was designed for the shaft, and, to ensure motion at the damper, a short extension was added to the test shaft as shown in Figure 21. Initially a squeeze film damper was used with some success, but the present discussion centers on a replacement elastomer damper. This damper consisted of six small elastomeric buttons deployed at 120° intervals in two rings, one of which is shown in Figure 22. The combined stiffness of the elastomer damper was designed to be 4000 lb/in. with a loss factor of 0.75 (selected as a conservative value for Viton 70). Figure 23 shows that this elastomeric damper lets the rotor run to 13,000 rpm without any problem from subsynchronous vibrations. This is about twelve times the speed at which intolerable subsynchronous vibrations were encountered when the power transmission shaft was hard mounted. Figure 24 shows a frequency spectrum at 13,000 rpm where the first critical subsynchronous vibrations are still less than 30 percent of the synchronous vibrations. Again, these results are considered impressive evidence of the ability of elastomeric dampers to control undesirable vibrations in flexible rotors.

Gas Bearing Mounted High-Speed Rotor

Striking success was achieved by flexibly mounting the gas bearings used to support a high-speed rotor required to run to over 120,000 rpm. In its hard-mounted configuration, this rotor encountered severe subsynchronous vibrations at about 280 Hz long before it reached its desired running speed. However, by flexibly mounting both gas bearings in O-rings, the rotor could be run all the way to its desired operating speed with only very small amplitude vibrations. The left-hand photograph of Figure 25 shows the 1.4 mil subsynchronous vibration orbit when the hard-mounted rotor was running at 108,600 rpm. The right-hand photograph shows the predominantly synchronous vibration orbit of 0.2 mil when

the O-ring mounted rotor was running at 114,600 rpm. These results are regarded as further strong evidence for the potential benefits of using elastomeric mounts to control instabilities.

CONCLUSIONS

With good material and component data, effective system and component design, and appropriate consideration for the application environment, elastomeric dampers hold considerable promise as simple low-cost devices for controlling undesirable vibrations in rotating machinery, both synchronous and subsynchronous.

REFERENCES

1. Chiang, T., Tessarzik, J.M., and Badgley, R.H., "Development of Procedures for Calculating Stiffness and Damping Properties of Elastomers in Engineering Applications, Part I: Verification of Basic Methods", NASA Report CR-120905, March 1972. Prepared by MTI for NASA-Lewis Research Center under Contract NAS3-15334.

2. Gupta, P.K., Tessarzik, J.M., and Cziglenyi, L., "Development of Procedures for Calculating Stiffness and Damping Properties of Elastomers in Engineering Applications, Part II: Elastomer Characteristics at Constant Temperature", NASA Report CR-134704, April 1974. Prepared by MTI for NASA-Lewis Research Center under Contract NAS3-15334.

3. Smalley, A.J., and Tessarzik, J.M., "Development of Procedures for Calculating Stiffness and Damping Properties of Elastomers in Engineering Applications, Part III: The Effects of Temperature, Dissipation Level and Geometry", NASA Report CR-134939, November 1975. Prepared by MTI for NASA-Lewis Research Center under Contract NAS3-15334, and NAS3-18546.

4. Darlow, M.S., and Smalley, A.J., "Development of Procedures for Calculating Stiffness and Damping Properties of Elastomers in Engineering Applications, Part IV: Testing of Elastomers under a Rotating Load", NASA Report CR-135355, November 1977. Prepared by MTI for NASA-Lewis Research Center under Contract NAS3-18546.

5. Smalley, A.J., Darlow, M.S., and Mehta, R.K., "Stiffness and Damping of Elastomeric O-Ring Bearing Mounts", NASA Report CR-135328, November 1977. Prepared by MTI for NASA-Lewis Research Center under Contract NAS3-19751.

6. Tecza, J.A., Darlow, M.S., Jones, S.W., Smalley, T.J., and Cunningham, R.E., "Elastomer Mounted Rotors an Alternative for Smooth Running Turbomachinery", ASME paper 78-GT-149, presented at the Gas Turbine Conference and Exhibit and Solar Energy Conference in San Diego, CA, March 12-15, 1979.

7. Darlow, M.S., and Smalley, A.J., "The Effects of Strain and Temperature on the Dynamic Properties of Elastomers", ASME paper 79-DET-57.

8. Tecza, J.A., Darlow, M.S., Smalley, A.J., and Cunningham, R.E., "Design of Elastomer Dampers for a High-Speed Flexible Rotor", ASME Paper 79DET88.

9. Zorzi, E.S., Burgess, G., and Cunningham, R., "Elastomer Damper Performance – A Comparison with a Squeeze Film for A Supercritical Power Transmission Shaft", ASME paper 80-GT-162.

TURBOSHAFT DYNAMIC SIMULATOR COMPARISON OF LOG DECREMENT FOR
POLYBUTADIENE AND VITON-70 WITH OPTIMUM DAMPING

(2nd Critical Speed; Stiffness = 100,000 1b/in.)

	B (lb-sec/in.)	δ
(1) OPTIMUM	100	0.965
(2) POLYBUTADIENE	7.2	0.075
(3) VITON-70	38	0.31

TABLE 1

BASE EXCITATION RESONANT MASS TEST SCHEMATIC

BELLOFRAM SEALS

MASS SUPPORT
AIR SPRING

MASS

AXIAL MOTION MASS
GUIDE SPOKES

BELLOFRAM
SEALS

PRELOAD
AIR SPRING

ELASTOMER SAMPLE

ϕ

Y

Y_0

VIBRATING TABLE
SURFACE

ELECTROMAGNETIC
SHAKER
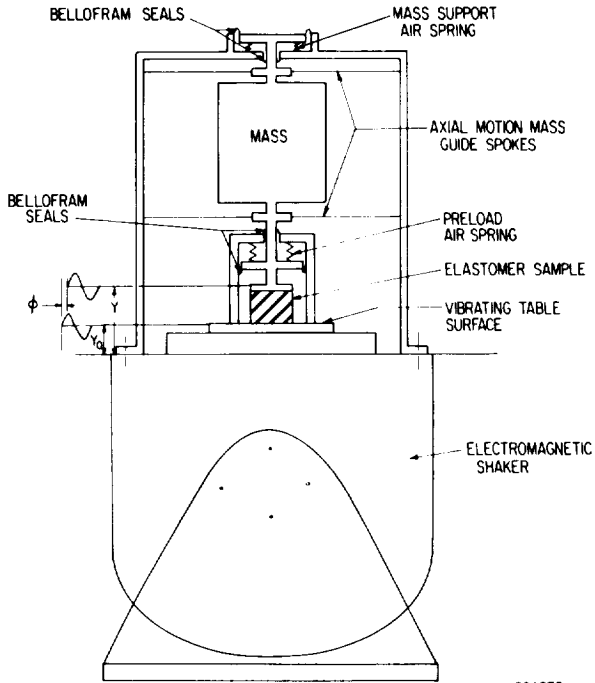
801378

Figure 1

SCHEMATIC OF COMPONENT GEOMETRIES TESTED

LOAD

WIDTH, b

LENGTH, x

THICKNESS, h

A SHEAR ELEMENT

ℓ

SPECIMEN

$2r_1$ $2r_2$

C. CARTRIDGE

LOAD

HEIGHT, h

DIAMETER, D

B COMPRESSION ELEMENT
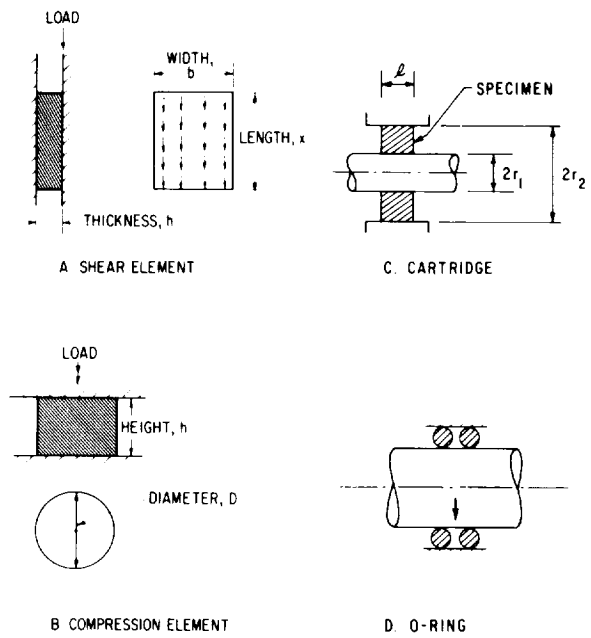
D. O-RING

801393

Figure 2

ILLUSTRATIVE TEST RESULTS: SHEAR SPECIMEN STIFFNESS, DAMPING VERSUS FREQUENCY

$K_1 = 1.355 \times 10^6 \, \omega^{.3009}$

$K_2 = 8.545 \times 10^5 \, \omega^{.1729}$

STIFFNESS AND DAMPING, N/m

FREQUENCY, HZ

801423

Figure 3

459
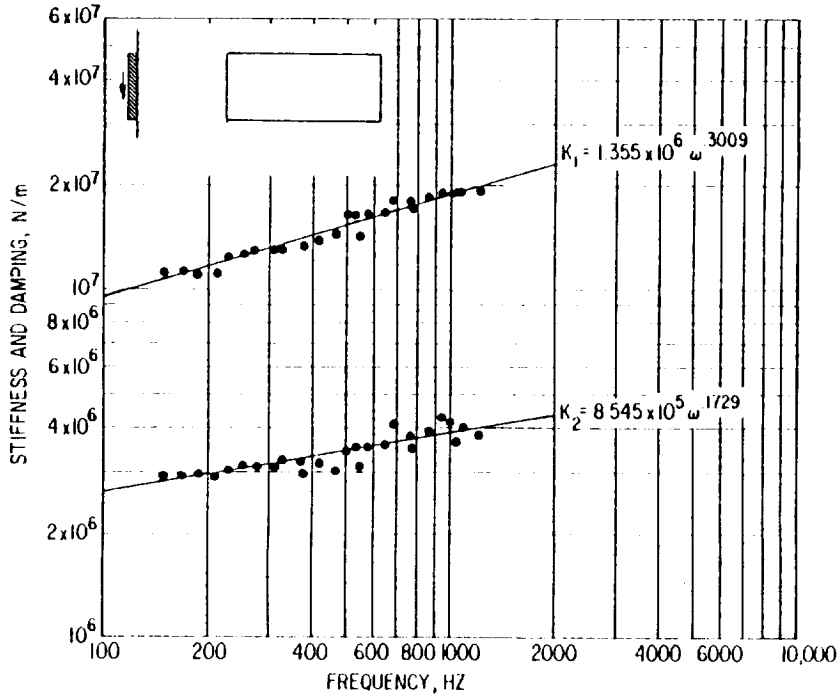
EFFECT OF DIAMETER TO HEIGHT RATIO ON CYLINDRICAL BUTTON STIFFNESS

$$K_2 = \frac{3G''A}{h}\left[1 + 2\left(\frac{d}{4h}\right)^2\right]$$

CORRELATION

$$K_2 = \frac{3G''A}{h}\left[1 + 2.244\left(\frac{d}{4h}\right)^2\right]$$
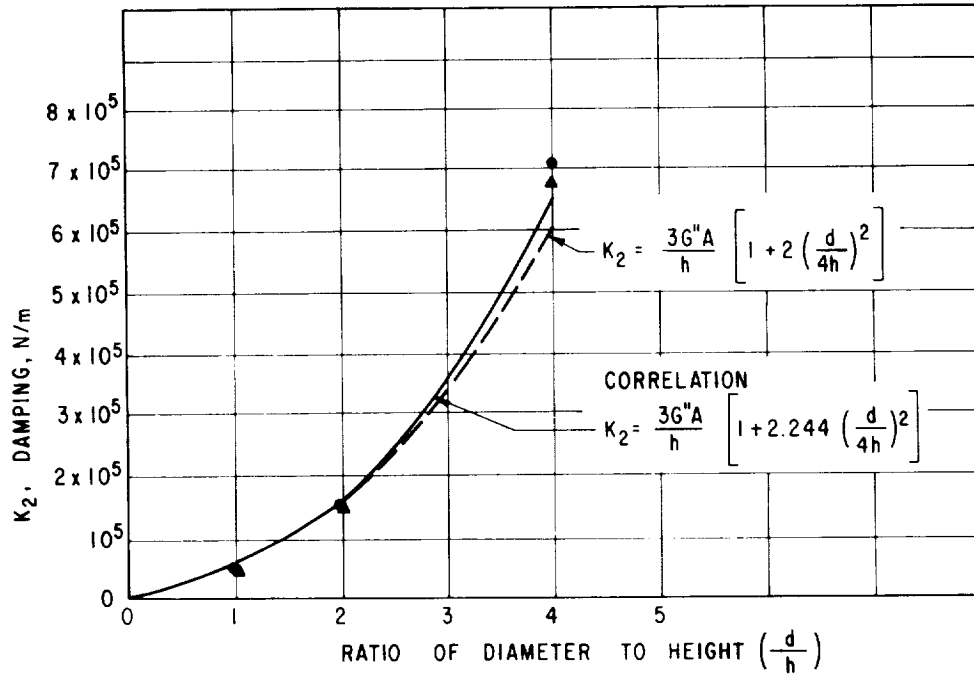
801438

Figure 4

O-RING STIFFNESS AND LOSS COEFFICIENT
FOR DIFFERENT MATERIALS
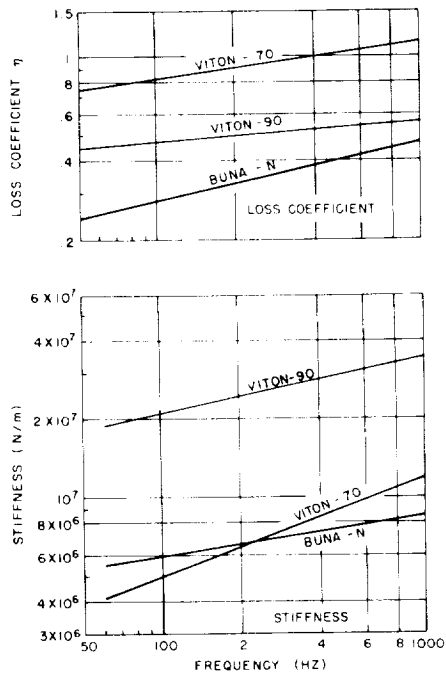
801452

Figure 5

O-RING STIFFNESS AND LOSS COEFFICIENT
FOR VITON-70 AT DIFFERENT TEMPERATURES

801467

Figure 6

460
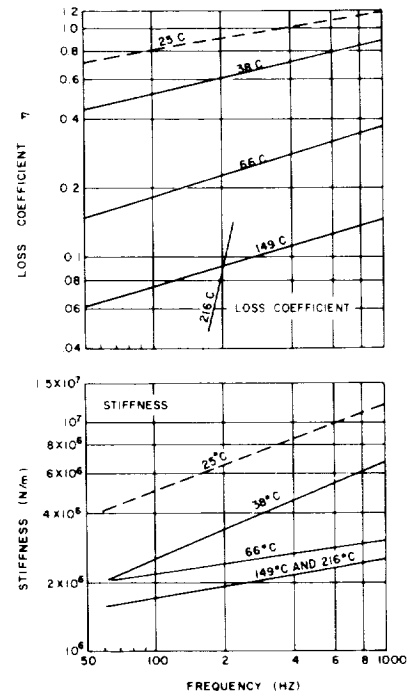
STIFFNESS AND LOSS COEFFICIENT VERSUS STRAIN FOR CYLINDRICAL BUTTONS IN COMPRESSION

STIFFNESS N/m

LOSS COEFFICIENT

STRAIN

Figure 7

792071

O-RING STIFFNESS AND LOSS COEFFICIENT FOR DIFFERENT AMPLITUDES

LOSS COEFFICIENT

7.62×10^{-6} m

25.4×10^{-6} m

127×10^{-6} m (5 MILS)

76×10^{-3}/F m

STIFFNESS

7.62×10^{-6} m (.3 MILS)

25.4×10^{-6} m (1 MIL)

76×10^{-3}/F m

127×10^{-6} m (5 MILS)

FREQUENCY (HZ)
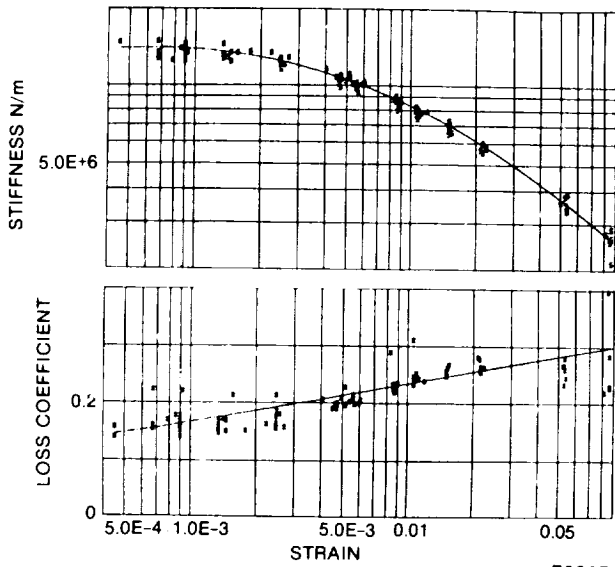
Figure 9

801235

AXIAL TEMPERATURE PROFILE IN CYLINDRICAL BUTTONS FOR COMPRESSION

TEMPERATURE (°C)

STRAIN = 0.083

STRAIN = 0.054

STRAIN = 0.022

STRAIN = 0.015

Figure 8

792072
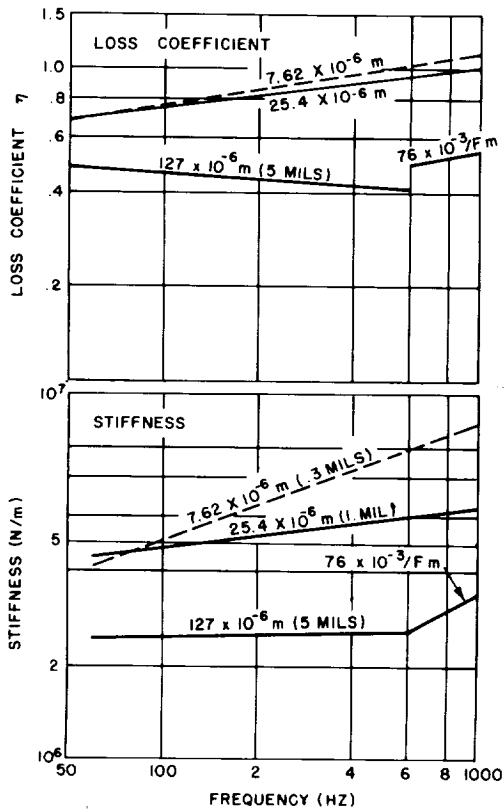
INFORMATION FLOW DIAGRAM FOR ROTORDYNAMICS — COMPONENT INTERACTION

BEARING CHARACTERISTICS

ENVIRONMENT

ROTOR MODEL

ANALYSIS FOR LOG DECREMENT OR RESPONSE

OPTIMUM BEARING SUPPORT STIFFNESS AND DAMPING

MATERIAL CANDIDATES AND ENVELOPE CONSTRAINTS

SENSITIVITY TO NON-OPTIMUM CHARACTERISTICS

COMPONENT ANALYSIS AND DESIGN SYNTHESIS

ALTERNATIVE CONFIGURATIONS AND CORRESPONDING COMPONENT CHARACTERISTICS

SELECTED CONFIGURATION AND ROTOR-SYSTEM DYNAMIC CHARACTERISTICS

● GEOMETRY, MATERIAL
● CRITICAL SPEED
● RESPONSE TO UNBALANCE
● STABILITY

801482

Figure 10

461

LOG DECREMENT VERSUS DAMPING COEFFICIENT: CYLINDRICAL BUTTONS

2. CRITICAL

1. CRITICAL

LOG DECREMENT

PEDESTAL DAMPING (LB-SEC/IN.)
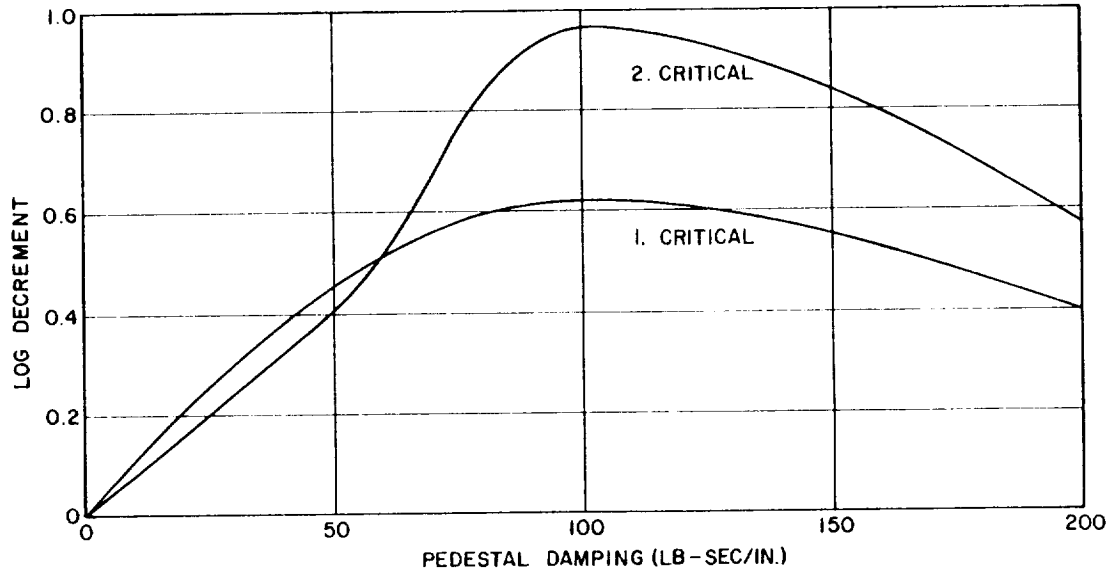
801057

Figure 11

PLOT OF CYLINDRICAL BUTTON STIFFNESS
VERSUS DIAMETER FOR DIFFERENT HEIGHTS

$.75 \, h_o$

h_o

$1.5 \, h_o$

STIFFNESS (lb/in)

BUTTON DIAMETER
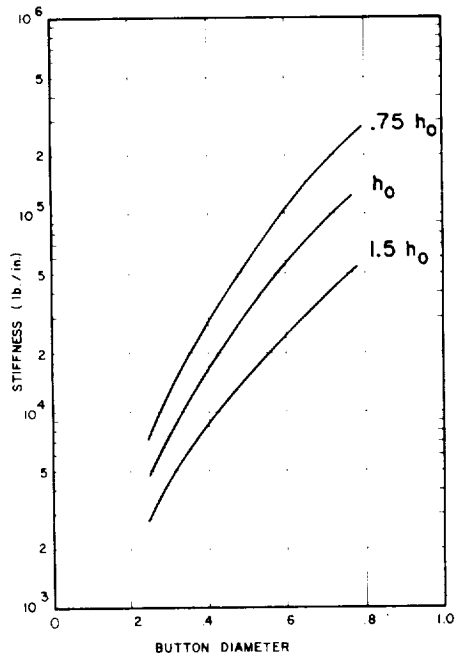
792521

Figure 12

SCHEMATIC OF
TURBOSHAFT ENGINE DYNAMIC SIMULATOR RIG

WEIGHT ADDED TO
DISC HERE FOR
SENSITIVITY RUNS

NONCONTACTING
DISPLACEMENT PROBES

3, 4   5, 6   7, 8   9, 10 11, 12   13, 14

1, 2

1, 3 etc.

2, 4 etc.

FRONT VIEW

ELASTOMER
BUTTONS

WEIGHT ADDED TO
SHAFT HERE FOR
SENSITIVITY RUNS

WEIGHT ADDITION
PLANES

791195

Figure 13

462
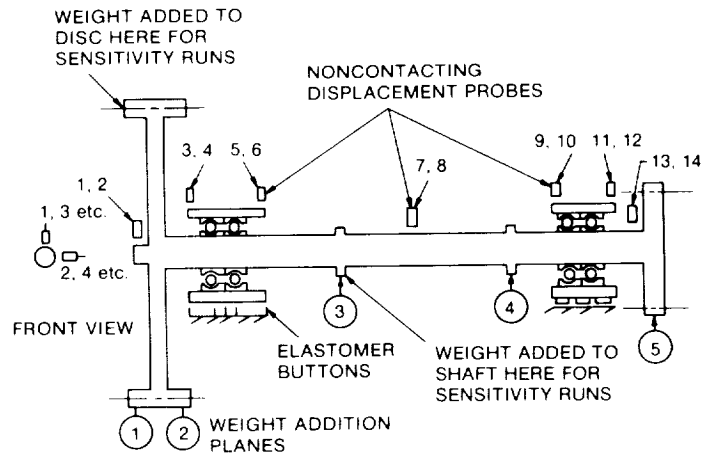
SCHEMATIC OF ELASTOMER DAMPER CONFIGURATION FOR TURBOSHAFT RIG
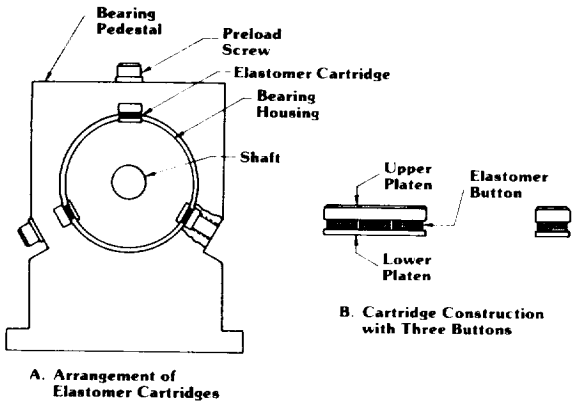
Figure 14

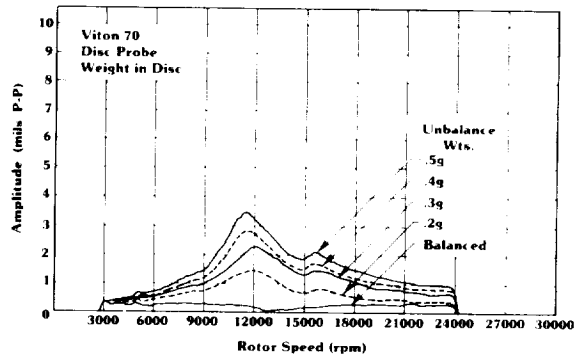## PREDICTED RESPONSE OF TURBOSHAFT RIG FOR VITON AND POLYBUTADIENE DAMPER
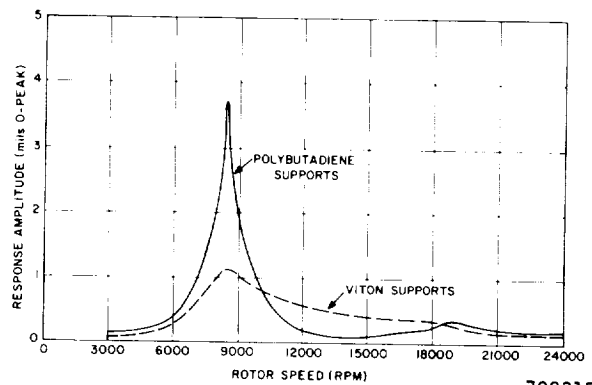
Figure 15

MEASURED RESPONSE OF TURBOSHAFT DAMPER ON HARD MOUNT
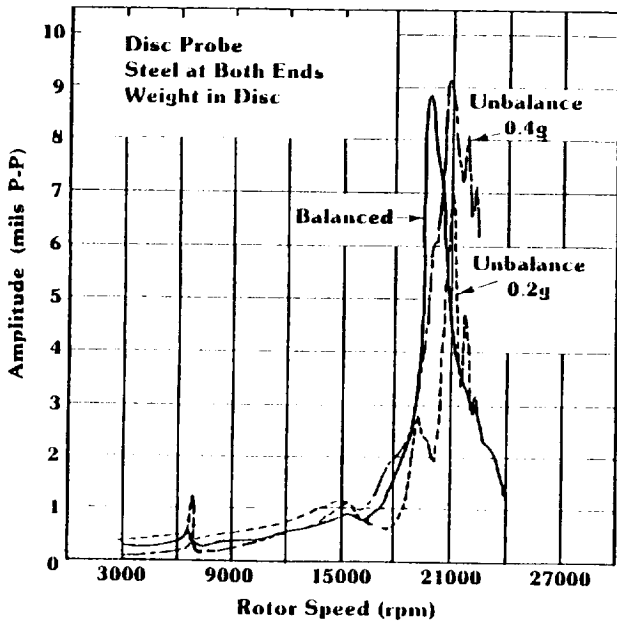
Figure 16

MEASURED RESPONSE OF TURBOSHAFT RIG ON VITON-70 DAMPER

Figure 17

463
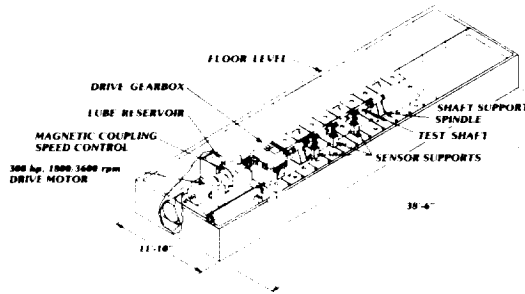
SCHEMATIC OF
SUPERCRITICAL SHAFT TEST RIG

FLOOR LEVEL

DRIVE GEARBOX
LUBE RESERVOIR
MAGNETIC COUPLING
SPEED CONTROL
300 hp, 1800-3600 rpm
DRIVE MOTOR

SHAFT SUPPORT
SPINDLE
TEST SHAFT
SENSOR SUPPORTS

38'-6"

11'-10"

801572

Figure 18

RESPONSE AMPLITUDE VERSUS SPEED;
SUPERCRITICAL SHAFT RIG WITHOUT DAMPER
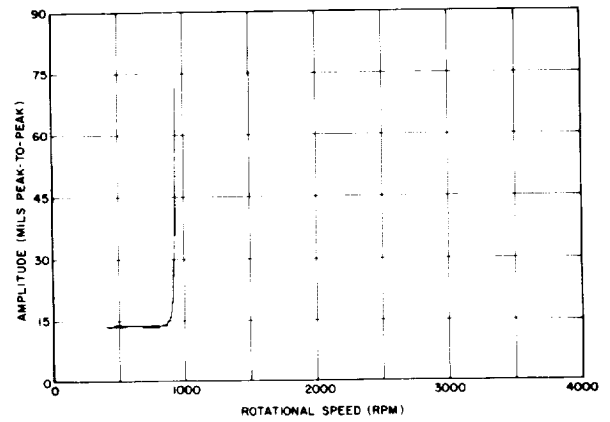
801587

Figure 19

FREQUENCY SPECTRUM;
SUPERCRITICAL SHAFT RUNNING ABOVE
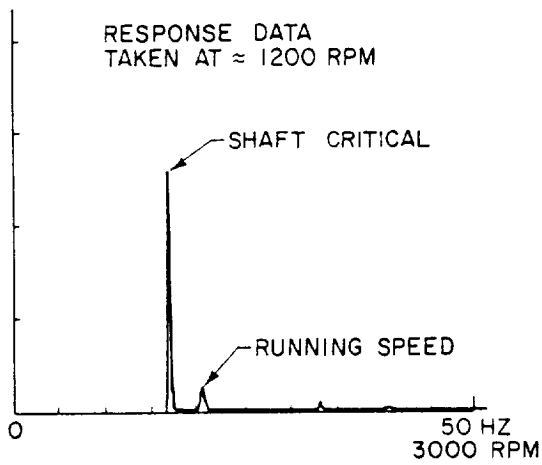### FIRST CRITICAL WITHOUT DAMPER

RESPONSE DATA
TAKEN AT ≈ 1200 RPM

SHAFT CRITICAL

RUNNING SPEED

0   50 HZ
                        3000 RPM

801542

Figure 20

SCHEMATIC SHOWING LOCATION OF
DAMPER ON SUPERCRITICAL SHAFT RIG

COUPLING   COUPLING

HARD-MOUNT
CONFIGURATION

TEST SHAFT

COUPLING   COUPLING   COUPLING

CONFIGURATION WITH
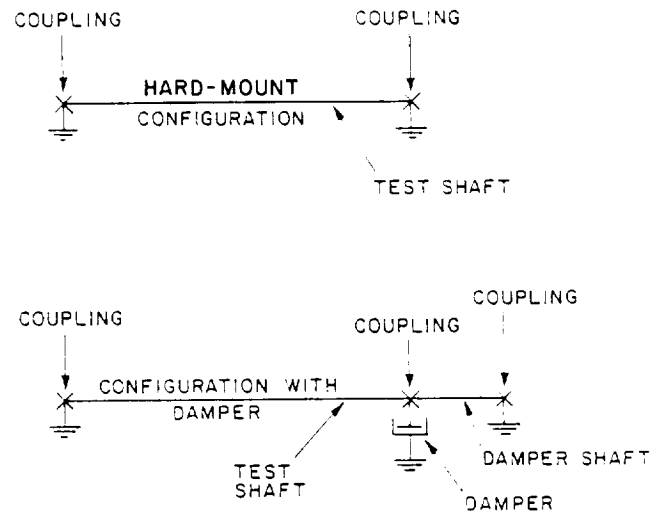DAMPER

TEST
SHAFT

DAMPER SHAFT

DAMPER

801557

Figure 21

464

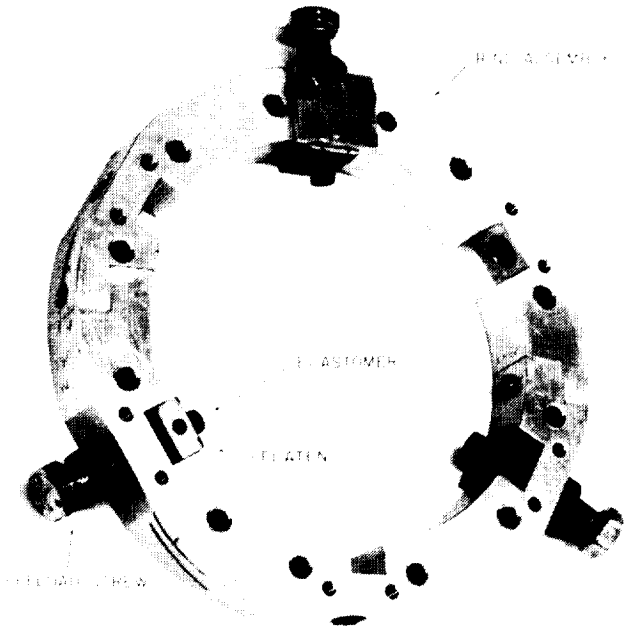PHOTO OF ELASTOMER DAMPER
FOR SUPERCRITICAL SHAFT

Figure 22

RESPONSE AMPLITUDE VERSUS SPEED;
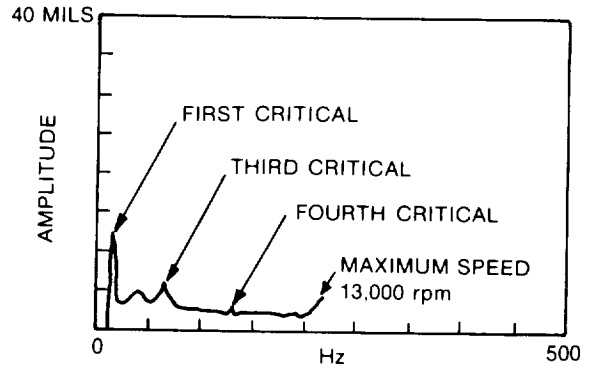SUPERCRITICAL SHAFT WITH
ELASTOMER DAMPER

Figure 23

792379

FREQUENCY SPECTRUM;
SUPERCRITICAL SHAFT RUNNING ABOVE
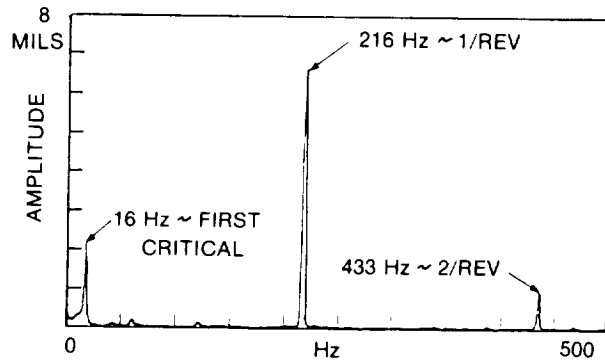FOURTH CRITICAL WITH ELASTOMER DAMPER

Figure 24

792377

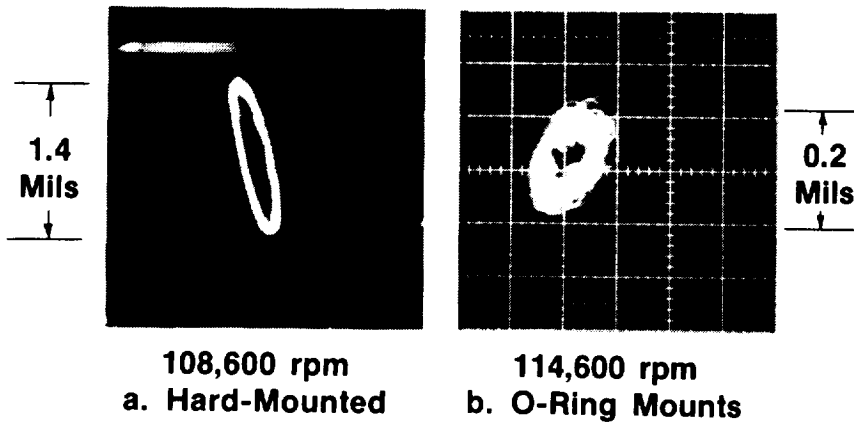COMPARISON OF ORBITS; GAS-BEARING ROTOR HARDMOUNTED AND ON O-RING MOUNTS

1.4
Mils

0.2
Mils

108,600 rpm
a. Hard-Mounted

114,600 rpm
b. O-Ring Mounts

Figure 25